Research article

Journal of RAMAN SPECTROSCOPY

Received: 20 February 2014 Revised: 23 May 2014 Accepted: 29 May 2014 Published online in Wiley Online Library: 3 July 2014

(wileyonlinelibrary.com) DOI 10.1002/jrs.4529

Raman spectroscopic characterization of CH_4 density over a wide range of temperature and pressure†

Linbo Shang,[a]* I-Ming Chou,[b,c] R. C. Burruss,[d] Ruizhong Hu[a] and Xianwu Bi[a]

The positions of the CH_4 Raman ν_1 symmetric stretching bands were measured in a wide range of temperature (from −180 °C to 350 °C) and density (up to 0.45 g/cm^3) using high-pressure optical cell and fused silica capillary capsule. The results show that the Raman band shift is a function of both methane density and temperature; the band shifts to lower wavenumbers as the density increases and the temperature decreases. An equation representing the observed relationship among the CH_4 ν_1 band position, temperature, and density can be used to calculate the density in natural or synthetic CH_4-bearing inclusions. Copyright © 2014 John Wiley & Sons, Ltd.

Keywords: CH_4 density; Raman spectroscopy; fused silica capillary capsule; high-pressure optical cell

Introduction

Raman spectroscopy has been used to provide information on both composition and internal pressure (or density) of fluid inclusions.[1–4] This information can be used to formulate the conditions for the formation of fluid inclusions and the geological environments for the formation of the host minerals. Methane-bearing inclusions exist in many geological environments; they were found, for example, in sedimentary basins,[5] low grade metamorphic rocks,[6] and mid-ocean ridge hydrothermal environments.[7,8] In order to quantitatively analyze the CH_4-bearing fluids, certain fundamental questions about the response of the Raman bands to the molecular environments of methane need to be answered. Composition, temperature, and pressure (or density) are important factors affecting molecular environments. Previous Raman work on methane has shown that the peak position of the C–H symmetric stretching band (ν_1) of methane shifts to lower wavenumbers with increasing pressure at near room temperature.[1–3,9–12] Lu *et al.*[3] developed a unified equation for the relationship between pressure and Raman peak position for CH_4 ν_1 band near room temperature, and this relationship can be applied in any laboratory. On the other hand, the temperature effect on the relationship between Raman CH_4 ν_1 peak position and pressure (or density) is not as well documented. Previous works studied the temperature effect on the shifts of CH_4 ν_1 peak position[1–3,13,14]; Lin *et al.*[1,2] gave the relationship among Raman CH_4 ν_1 peak position and temperature (0.3–22 °C) and pressure and showed that the peak position shifted to higher wavenumbers with temperature increase, while Lu *et al.*[3] did not find an obvious temperature effect on the Raman CH_4 ν_1 peak position in their band position *versus* density plot.

In this study, we used high-pressure optical cell (HPOC)[15] and also fused silica capillary capsule (FSCC)[16] methods to collect Raman spectra of methane at densities up to 0.45 g/cm^3 and temperatures from −180 °C to 350 °C. These new measurements are used to construct a relationship among Raman CH_4 ν_1 peak position, temperature, and density of methane over a wide range of temperature and density.

Method

Experimental apparatus and procedures

High-pressure optical cell

An HPOC, in combination with a Linkam heating–cooling stage (to be described in the succeeding text), was used for our Raman spectroscopic study of a single phase of CH_4 in isothermal experiments. The experimental apparatus and procedures are identical to those employed by Lu *et al.*[3] and Wang *et al.*[4] The HPOC (Fig. 1 of Chou *et al.*[15]) was constructed from a fused silica capillary with round cross-section (Polymicro Technologies, LLC, http:// polymicro.com) with 300 μm OD, 100 μm ID, and about 18 cm length. One end of the tube was sealed with a hydrogen flame, and the other (open) end was cemented to the inside of a stainless steel high-pressure capillary tube (1.59 mm OD, 0.76 mm ID, and 30 mm length) with epoxy. The steel tube was connected to a pressurization system with a sleeve-gland assembly and a high-pressure valve (HIP, 15-15AF1, High pressure Equipment Company). The pressure in the cell was maintained with CH_4 in the pressure line and could be adjusted by using a pressure generator (HIP Model No. 37-6-30). The pressure was measured by a Setra 204D digital pressure transducer (accurate

* *Correspondence to: Linbo Shang, State Key Laboratory of Ore Deposit Geochemistry, Institute of Geochemistry, Chinese Academy of Sciences, Guiyang 550002, China. E-mail: shanglinbo@vip.gyig.ac.cn*

† *This article has been contributed by US Government employees and their work is in the public domain in the USA.*

a *State Key Laboratory of Ore Deposit Geochemistry, Institute of Geochemistry, Chinese Academy of Sciences, Guiyang 550002, China*

b *US Geological Survey, 954 National Center, Reston, VA 20192, USA*

c *Laboratory for Experimental Study Under Deep-sea Extreme Conditions, Sanya Institute of Deep-sea Science and Engineering, Chinese Academy of Sciences, Sanya 572000, China*

d *US Geological Survey, 956 National Center, Reston, VA 20192, USA*

Journal of RAMAN SPECTROSCOPY

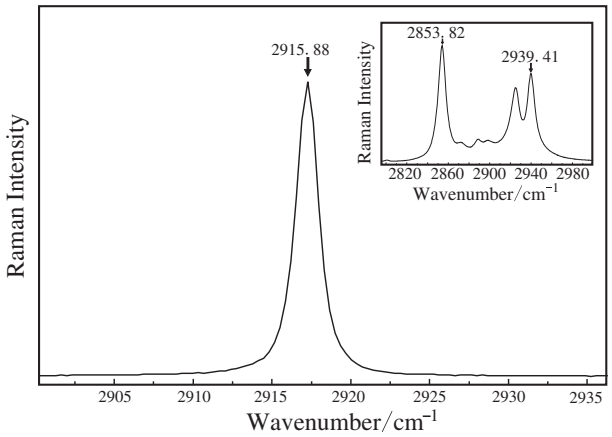

Figure 1. A Raman spectrum of CH_4, showing the peak position of the C–H symmetric stretching ν_1 band. The insert shows the spectrum of cyclohexane with well-defined peak positions at 2853.82 and 2939.41 cm^{-1} that bracket ν_1 band of CH_4 and were used to calibrate the peak position of CH_4 ν_1 band.

to ± 0.14%). After evacuating the pressure line and the HPOC, the system was flushed with CH_4 (99.99% purity, Air products, Inc.) before loading a sample. The sealed-end section of the tube was inserted into the sample chamber of the heating–cooling stage (CAP500, Linkam Scientific Instruments Ltd.; refer in the succeeding text) and placed near the center of the window of the heating–cooling stage, where the temperature could be controlled and read with a high accuracy 100-ohm platinum resistor. The Raman spectrum was collected at a fixed temperature and at pressures up to 68.87 MPa (the safe pressure limit for HPOC). The measured temperature and pressure were used to calculate the CH_4 density based on the NIST Chemistry WebBook (Available from: http://webbook.nist.gov/chemistry).

Fused silica capillary capsule

Fused silica capillary capsules (300 μm OD, 100 μm ID, and about 15 cm length) were prepared to contain pure CH_4, using the sample-loading system of Chou *et al.*[16] To construct a FSCC, one end of the silica tube was sealed with a hydrogen flame, and the open end of the tube was connected to a pressure line. The line and the silica tube were flushed twice with gaseous CH_4 after evacuation. The line and the silica tube were then pressurized with CH_4 to slightly less than 0.2 MPa, and liquid or solid CH_4 was precipitated by immersing the closed end of the tube in liquid nitrogen. The system was then evacuated, and the open end of the tube was sealed with a hydrogen flame while the closed end was still immersed in liquid nitrogen. The density of CH_4 in the FSCC was controlled by the CH_4 pressure, freezing time, and the length of the sealed capsule. A CH_4 sample in a FSCC was used in this study with a bulk density of 0.200 g/cm^3, which was determined by the measured homogenization temperature of −83.12 °C. Raman spectra were collected at fixed temperatures from −180 to −86 °C for both liquid and the coexisting vapor phase in a Linkam CAP500 heating–cooling stage. The fixed temperature was then used to calculate the densities of the liquid phase and the coexisting vapor phase based on the NIST chemistry WebBook.

LINKAM heating–cooling stage

A LINKAM CAP500 heating–cooling stage, which consists of a stage, a T95 system controller, and a liquid nitrogen cooling system, was used to control sample temperatures in both the HPOC and FSCC.[17] The stage was custom-designed for the HPOC and FSCC. HPOC can be directly placed in a slot in a silver heater block and covered by a silver cover with two screws. FSCC can be placed on a quartz sample carrier plate that was mounted to the sample holder to give a maximum of 25 mm of movement. The silver heater block can rapidly heat and cool in the range of −196 to 500 °C at a rate from 0.1 to 50 °C/min. The temperature sensor mounted in the silver block is a high accuracy 100 ohm platinum resistor to 1/10th Din Class A (CAP500 User Guide). The temperature measuring system was calibrated with the triple points of H_2O (0.0 °C), CO_2 (−56.56 °C), butane (−138.55 °C), and methane (−182.48 °C), the melting point of $NaNO_3$ (306.80 °C), the eutectic temperature of NaCl solution (−21.20 °C), and the critical temperature of H_2O (374.15 °C). The reported temperature is accurate to ±0.1 °C near room temperature (from −50 to 100 °C), ±0.2 °C at −138 °C and 307 °C, and ±1 °C at the triple point of methane (−182.48 °C).

Collection of Raman spectra and calibration of methane peak position

Raman spectra of methane were acquired using a JY/Horiba LabRam HR Raman system, with 532.06 nm (frequency doubled Nd:YAG) laser excitation, a 40× Olympus objective with 0.25 numerical aperture, and a 1800 grooves/mm grating, which has a spectral precision of about 1 cm^{-1}. Approximately 20 mW laser light was focused on a central level of the horizontal tube to generate CH_4 Raman signals during the measurement. As shown in Fig. 1, spectra were collected in a single window between 2850 and 3100 cm^{-1}, which covers the peak of CH_4 around 2918 cm^{-1}, and two reference peaks of cyclohexane (2853.815 and 2939.412 cm^{-1}) that were calibrated based on the Ne emission lines at 626.649 and 630.479 nm, which correspond to 2836.976 and 2933.916 cm^{-1}, respectively. The measured spectra for CH_4 and cyclohexane were fitted with the program PeakFit V. 4.0 (AISN Software Inc.), using Gaussian functions, no smoothing was applied to the spectra before peak fitting procedures, and the resolution can be enhanced to 0.03 cm^{-1} by using a curve fitting technique.[18]

The separation between the 2853.815 and 2939.412 cm^{-1} peaks of cyclohexane was used to calibrate the peak position of CH_4. Reference spectra of cyclohexane were collected at the beginning, during, and the end of the analytical session. The real Raman peak positions (ν_{real}) of the C–H symmetric stretching band (ν_1) of methane were derived from the measured peak position of the C–H symmetric stretching band ($\nu_{measured}$), the measured peak position of cyclohexane ($\nu_{cyclohexane}$) for the 2853.815 cm^{-1} band, and the measured separation between the two peaks of cyclohexane ($\Delta_{cyclohexane}$) by the following relationship:

$$\nu_{real}\left(cm^{-1}\right) = (2939.412\text{-}2853.815)/\,\Delta_{cyclohexane} * \left(\nu_{measured} - \nu_{cyclohexane}\right) + 2853.815 \quad (1)$$

Results and discussion

The calibrated methane ν_1 peak positions at various temperatures and pressures collected in an HPOC and a FSCC were listed in Tables 1 and 2, respectively. Results are represented by Fig. 2 and the following equation, which was obtained through a polynomial regression analysis (using the software 1stOpt):

Table 1. Calibrated methane ν_1 peak positions at various temperatures and pressures in an HPOC

T/°C	P/MPa	*Density/g-cm^{-3}	$\Delta_{cyclohexane}$	$\nu_{cyclohexane}$	$\nu_{measured}$	Shift/cm^{-1}	**Phase
100	5.566	0.02973	86.02	2854.06	2918.18	2917.62	SF(V)
100	7.566	0.040772	86.02	2854.06	2917.88	2917.32	SF(V)
100	9.821	0.053332	86.02	2854.06	2917.55	2916.99	SF(V)
100	11.372	0.061988	86.02	2854.06	2917.32	2916.76	SF(V)
100	13.372	0.073091	86.02	2854.06	2917.04	2916.49	SF(V)
100	15.772	0.08623	86.02	2854.06	2916.73	2916.18	SF(V)
100	17.676	0.096425	86.02	2854.06	2916.45	2915.90	SF(V)
100	20.841	0.11278	86.02	2854.06	2916.08	2915.53	SF(V)
100	24.310	0.12964	86.02	2854.06	2915.67	2915.12	SF(V)
100	27.828	0.14584	86.02	2854.06	2915.32	2914.77	SF(V)
100	30.945	0.15843	86.02	2854.06	2915.03	2914.49	SF(V)
100	34.097	0.17051	86.02	2854.06	2914.74	2914.20	SF(L)
100	37.490	0.18246	86.02	2854.06	2914.48	2913.94	SF(L)
100	42.000	0.19681	86.02	2854.06	2914.22	2913.68	SF(L)
100	45.462	0.20678	86.02	2854.06	2914.01	2913.47	SF(L)
100	49.731	0.21799	86.02	2854.06	2913.77	2913.23	SF(L)
100	51.710	0.22283	86.02	2854.06	2913.68	2913.14	SF(L)
22	0.041	0.000271	85.94	2854.26	2918.91	2918.21	SF(V)
22	0.117	0.000768	85.94	2854.26	2918.93	2918.23	SF(V)
22	0.428	0.002816	85.94	2854.26	2918.85	2918.15	SF(V)
22	0.986	0.006561	85.94	2854.26	2918.77	2918.07	SF(V)
22	1.766	0.011912	85.94	2854.26	2918.59	2917.89	SF(V)
22	3.662	0.025568	85.94	2854.26	2918.30	2917.60	SF(V)
22	8.441	0.063877	85.94	2854.26	2917.24	2916.54	SF(V)
22	14.069	0.11304	85.94	2854.26	2915.97	2915.28	SF(V)
22	17.938	0.14488	85.94	2854.26	2915.18	2914.49	SF(V)
22	24.255	0.18719	85.94	2854.26	2914.17	2913.49	SF(L)
22	29.945	0.21551	85.94	2854.26	2913.52	2912.84	SF(L)
22	36.207	0.23923	85.94	2854.26	2913.04	2912.36	SF(L)
22	42.434	0.25774	85.94	2854.26	2912.68	2912.00	SF(L)
22	52.634	0.28123	85.94	2854.26	2912.28	2911.60	SF(L)
22	56.331	0.2883	85.94	2854.26	2912.17	2911.49	SF(L)
22	60.703	0.29595	85.94	2854.26	2912.07	2911.39	SF(L)
−50	0.103	0.000898	86.09	2854.13	2918.93	2918.24	SF(V)
−50	0.255	0.002232	86.09	2854.13	2918.89	2918.20	SF(V)
−50	1.641	0.015374	86.09	2854.13	2918.47	2917.79	SF(V)
−50	2.786	0.027842	86.09	2854.13	2918.08	2917.40	SF(V)
−50	4.531	0.050932	86.09	2854.13	2917.37	2916.69	SF(V)
−50	6.269	0.081645	86.09	2854.13	2916.47	2915.80	SF(V)
−50	7.069	0.099512	86.09	2854.13	2915.96	2915.29	SF(V)
−50	7.731	0.11622	86.09	2854.13	2915.57	2914.90	SF(V)
−50	8.503	0.13715	86.09	2854.13	2914.99	2914.33	SF(V)
−50	9.138	0.15421	86.09	2854.13	2914.60	2913.94	SF(V)
−50	10.186	0.17921	86.09	2854.13	2913.99	2913.33	SF(L)
−50	11.434	0.20226	86.09	2854.13	2913.41	2912.76	SF(L)
−50	12.600	0.21851	86.09	2854.13	2913.04	2912.39	SF(L)
−50	14.076	0.23428	86.09	2854.13	2912.69	2912.04	SF(L)
−50	15.172	0.24368	86.09	2854.13	2912.46	2911.81	SF(L)
−50	16.628	0.25408	86.09	2854.13	2912.24	2911.59	SF(L)
−50	17.993	0.26231	86.09	2854.13	2912.06	2911.41	SF(L)
−50	19.490	0.2701	86.09	2854.13	2911.90	2911.25	SF(L)
−50	21.552	0.27929	86.09	2854.13	2911.71	2911.07	SF(L)
−50	23.683	0.28742	86.09	2854.13	2911.55	2910.91	SF(L)
−50	26.483	0.29659	86.09	2854.13	2911.39	2910.75	SF(L)
−50	29.455	0.30459	86.09	2854.13	2911.22	2910.58	SF(L)
−50	32.324	0.31203	86.09	2854.13	2911.15	2910.51	SF(L)
−50	35.821	0.31971	86.09	2854.13	2911.02	2910.38	SF(L)

(Continues)

Table 1. (Continued)

T/°C	P/MPa	*Density/g-cm^{-3}	$\Delta_{cyclohexane}$	$\nu_{cyclohexane}$	$\nu_{measured}$	Shift/cm^{-1}	**Phase
−50	39.600	0.32697	86.09	2854.13	2910.90	2910.26	SF(L)
−50	44.200	0.33484	86.09	2854.13	2910.79	2910.15	SF(L)
−50	49.200	0.34243	86.09	2854.13	2910.70	2910.06	SF(L)
−50	53.255	0.34799	86.09	2854.13	2910.63	2909.99	SF(L)
−50	58.938	0.35509	86.09	2854.13	2910.58	2909.94	SF(L)
−150	0.255	0.40504	86.02	2854.06	2907.96	2907.45	L
−150	7.441	0.41294	86.02	2854.06	2907.89	2907.38	L
−150	15.807	0.4208	86.02	2854.06	2907.87	2907.36	L
−150	28.021	0.43054	86.02	2854.06	2907.88	2907.37	L
−150	44.924	0.44181	86.02	2854.06	2907.93	2907.42	L
−150	60.531	0.4507	86.02	2854.06	2907.98	2907.47	L
0	7.062	0.059461	86.00	2854.15	2917.25	2916.62	SF(V)
50	7.062	0.045798	86.00	2854.15	2917.77	2917.14	SF(V)
100	7.062	0.037981	86.00	2854.15	2918.1	2917.47	SF(V)
150	7.062	0.032714	86.00	2854.15	2918.33	2917.69	SF(V)
200	7.062	0.028853	86.00	2854.15	2918.47	2917.83	SF(V)
250	7.062	0.025871	86.00	2854.15	2918.63	2917.99	SF(V)
300	7.062	0.023484	86.00	2854.15	2918.68	2918.04	SF(V)
350	7.062	0.021522	86.00	2854.15	2918.80	2918.16	SF(V)
−60	7.641	0.15025	86.07	2854.12	2914.51	2913.87	SF(V)
−40	10.324	0.15006	86.07	2854.12	2914.60	2913.96	SF(V)
−20	13.007	0.15003	86.07	2854.12	2914.73	2914.09	SF(V)
0	15.683	0.15002	86.07	2854.12	2914.85	2914.21	SF(V)
20	18.352	0.15005	86.07	2854.12	2914.94	2914.30	SF(V)
50	22.331	0.15005	86.07	2854.12	2915.09	2914.45	SF(V)
100	28.890	0.15001	86.07	2854.12	2915.31	2914.67	SF(V)
150	35.393	0.15003	86.07	2854.12	2915.52	2914.88	SF(V)
200	41.821	0.15002	86.07	2854.12	2915.72	2915.08	SF(V)
250	48.186	0.15001	86.07	2854.12	2915.87	2915.23	SF(V)
300	54.510	0.15003	86.07	2854.12	2915.90	2915.26	SF(V)
350	60.772	0.15001	86.07	2854.12	2916.12	2915.47	SF(V)
−80	5.552	0.23002	86.02	2854.06	2912.36	2911.83	SF(L)
−60	10.897	0.23007	86.02	2854.06	2912.45	2911.92	SF(L)
−40	16.400	0.23004	86.02	2854.06	2912.6	2912.07	SF(L)
−20	21.945	0.23002	86.02	2854.06	2912.79	2912.26	SF(L)
0	27.490	0.23000	86.02	2854.06	2912.96	2912.43	SF(L)
20	33.028	0.23003	86.02	2854.06	2913.08	2912.54	SF(L)
40	38.524	0.23001	86.02	2854.06	2913.24	2912.70	SF(L)
60	43.993	0.23001	86.02	2854.06	2913.43	2912.89	SF(L)
80	49.428	0.23002	86.02	2854.06	2913.5	2912.96	SF(L)
100	54.807	0.22998	86.02	2854.06	2913.67	2913.13	SF(L)
20	68.869	0.31002	86.07	2854.14	2911.89	2911.25	SF(L)
−40	36.924	0.31002	86.07	2854.14	2911.22	2910.58	SF(L)
−60	26.007	0.31006	86.07	2854.14	2911.02	2910.38	SF(L)
−80	14.966	0.31001	86.07	2854.14	2910.77	2910.13	SF(L)

HPOC, high-pressure optical cell.

* Calculated from NIST chemistry WebBook.

** L is liquid phase, SF(V) is supercritical fluid with vapour like density (<0.16266 g-cm^{-3}), and SF(L) is supercritical fluid with liquid like density (>0.16266 g-cm^{-3}).

$\nu_{measured}$ is the measured peak position of the C–H symmetric stretching band of CH_4.

$\nu_{cyclohexane}$ is the measured peak position of cyclohexane for the 2853.815 cm^{-1} band.

$\Delta_{cyclohexane}$ is the measured separation between the two peaks of cyclohexane (see text).

$$\rho = p_{00} + p_{10}\times T + p_{01}\times \nu_1 + p_{20}\times T^2 + p_{11}\times T\times \nu_1 + p_{02}\times {\nu_1}^2 \quad (2)$$

where ν_1 is the Raman peak shift in cm^{-1}, T is the temperature in °C, and ρ is the density of CH_4 in g/cm^3. The fitted coefficients for Eqn (2) are listed in Table 3, and the root-mean-square error of

Table 2. Calibrated methane ν_1 peak positions for the vapor and coexisting liquid phases in a FSCC, which contains pure CH_4 with a bulk density of 0.2 g/cm^3

T/°C	*P*/MPa*	Liquid					Vapor				
		Density/ g-cm^{-3}*	$\Delta_{cyclohexane}$	$\nu_{cyclohexane}$	$\nu_{measured}$	Shift/cm^{-1}	Density/ g-cm^{-3}*	$\Delta_{cyclohexane}$	$\nu_{cyclohexane}$	$\nu_{measured}$	Shift/cm^{-1}
−180	0.016	0.4482	86.07	2854.09	2906.86	2906.30	—	—	—	—	—
−170	0.047	0.43451	86.12	2854.12	2907.33	2906.70	—	—	—	—	—
−160	0.114	0.42018	86.12	2854.12	2907.59	2906.96	—	—	—	—	—
−150	0.238	0.40502	86.12	2854.12	2907.97	2907.34	—	—	—	—	—
−140	0.442	0.38879	86.12	2854.12	2908.31	2907.68	0.007116	86.07	2854.09	2918.54	2917.91
−130	0.752	0.37111	86.12	2854.12	2908.72	2908.08	0.011848	86.07	2854.09	2918.43	2917.80
−120	1.196	0.35144	86.07	2854.13	2909.16	2908.54	0.018813	86.07	2854.09	2918.13	2917.50
−110	1.803	0.32876	86.07	2854.13	2909.79	2909.17	0.029056	86.07	2854.09	2917.75	2917.13
−100	2.604	0.30098	86.07	2854.13	2910.44	2909.82	0.044717	85.94	2854.23	2917.35	2916.68
−95	3.090	0.28364	86.07	2854.13	2910.87	2910.24	0.056136	85.94	2854.23	2917.07	2916.40
−90	3.640	0.26166	86.07	2854.13	2911.35	2910.72	—	—	—	—	—
−88	3.880	0.25044	86.07	2854.13	2911.62	2910.99	—	—	—	—	—
−86	4.133	0.23641	86.07	2854.13	2911.93	2911.30	—	—	—	—	—

FSCC, fused silica capillary capsule.

* Calculated from NIST chemistry WebBook.

$\nu_{measured}$ is the measured peak position of the C–H symmetric stretching band of CH_4.

$\nu_{cyclohexane}$ is the measured peak position of cyclohexane for the 2853.815 cm^{-1} band.

$\Delta_{cyclohexane}$ is the measured separation between the two peaks of cyclohexane (see text).

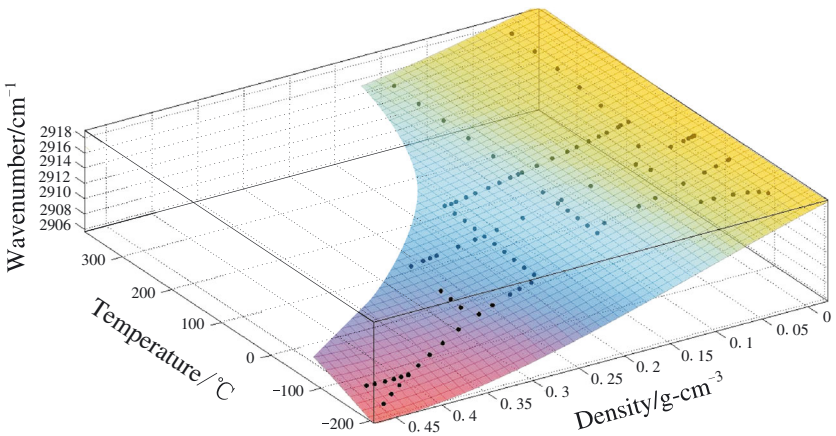

Figure 2. Relationship among methane ν_1 peak positions, temperature, and density for the temperatures from −180 to 350 °C and the densities from 0.0007 to 0.45 g/cm^3 (the figure was plotted by using the software MATLAB).

Eqn (2) is 0.008 g/cm^3 with an R^2 of 0.9960. Equation (2) can be used to calculate methane density in a sample fluid with measured Raman shift of the CH_4 ν_1 peak position at a fixed temperature. Almost the same equation was obtained through MATLAB software with similar accuracy.

The uncertainty in the measurements of the associated peak positions is estimated to be about 0.03 cm^{-1}. The total error in the calculated density of methane is about ±0.01 g/cm^3, when using Eqn (2).

Temperature effect on the shifts of CH_4 ν_1 peak position

To investigate the temperature effect on the Raman spectra of CH_4, a HPOC was used to collect Raman spectra of CH_4 from −60 to 350 °C at a constant density of 0.15 g/cm^3, from −80 to 100 °C at 0.23 g/cm^3, and from −80 to 20 °C at 0.31 g/cm^3 (Table 1). At a constant density, as clearly shown in Fig. 3, the CH_4 ν_1 peak position shifts to higher wavenumbers as the temperature increases. Also, this temperature effect is larger at higher density, with only about 0.2 cm^{-1} shift at near zero density between −100 and 300 °C. Figure 4 also shows the obvious trend of temperature dependence at −50, 22, and 100 °C. The trend is consistent with that of Echargui and Marsault-Herail[14] and Lin *et al.*[1,2] Therefore, the temperature effect must be considered when Raman shifts are used to calculate methane density or pressure.

Shift of CH_4 ν_1 peak position *versus* the density of methane

Figure 4 shows the relationship between CH_4 ν_1 peak position and density of CH_4 at fixed temperatures of −50, 22, and 100 °C;

Table 3. Fitting parameters for Eqn. (2)

P_{00}	13260.2997734257
P_{10}	0.159909924698094
P_{01}	−9.0579957183101
P_{20}	−8.23392651807174E-8
P_{11}	−5.47854804748698E-5
P_{02}	0.00154684331421227

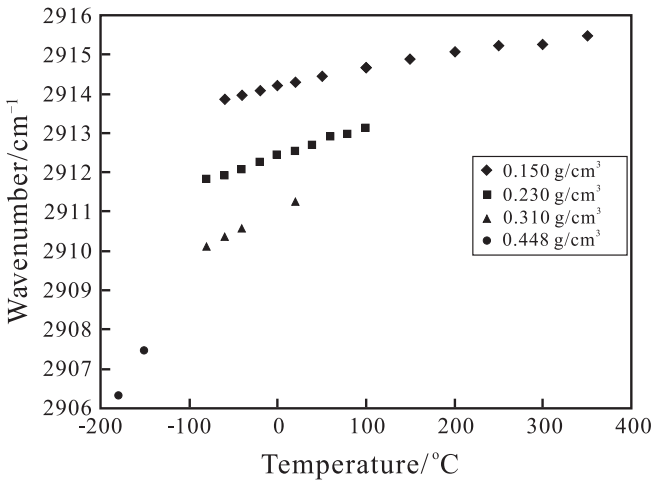

Figure 3. Relationship between methane ν_1 peak positions and temperature at constant density.

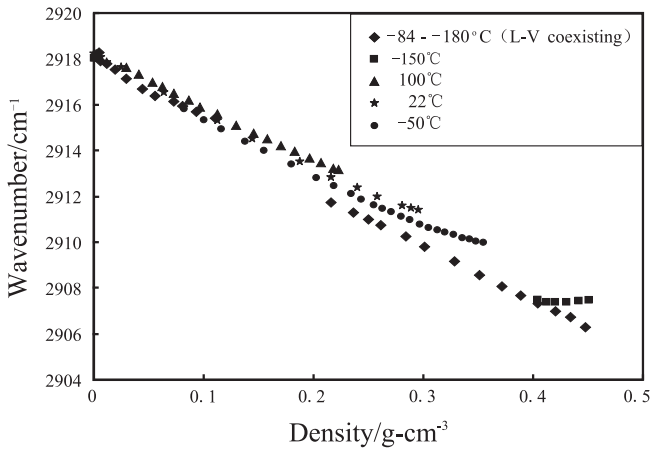

Figure 4. Methane ν_1 peak positions as a function of density at different temperatures.

the Raman peak position shifts to lower wavenumbers with increasing density at isothermal conditions. As shown in Fig. 5, our results at 22 °C agree well with previous studies,[2,3,11,12,19] especially those of Lu *et al.*[3] In this plot, D instead of ν_1 was used as a variable to eliminate the systematic discrepancies among the published sets of measurements from different Raman laboratories. As described by Lu *et al.*,[3] $D = \nu_p - \nu_0$, the difference between the peak positions at elevated density (ν_p) and near zero density ($\nu_0 = 2918.30\ cm^{-1}$ in this study).

At high density, the peak position shifts to slightly higher wavenumbers at −150 °C (Fig. 4). This change in slope in the ν_1 peak position *versus* density plot was previously observed at

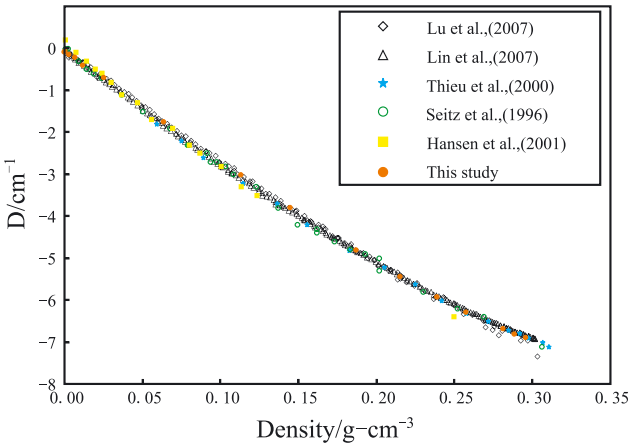

Figure 5. The relationship between D and density at 22 °C from this study, which agrees well with other published values at near room temperatures. $D = \nu_p - \nu_0$, the difference between the peak positions at elevated density (ν_p) and near zero density (ν_0), as defined by Lu *et al.*[3]

higher pressures (and density) by Fabre and Couty,[9] reflecting a change of molecular environment. This shift can be explained by a hard sphere theoretical model of vibrational frequency shifts due to the interactions of attractive and repulsive forces between molecules. At lower densities, van der Waals-type attractive forces dominate and, at higher densities, repulsive forces become more important.[20,21]

In this study, we also used an even more convenient way to calibrate a Raman spectrometer for CH_4 density measurements using CH_4 standards with various densities available in a single FSCC at fixed temperatures; this method has been successfully applied to the pure CO_2 system.[22] *In situ* Raman spectra were collected at fixed temperatures between the triple-point temperature of CH_4 at −182.46 °C and its critical temperature at −82.59 °C for both liquid and the coexisting vapor phases with CH_4 densities ranging from 0.00716 to 0.4482 g/cm^3 in a FSCC, which contains CH_4 with a bulk density of 0.200 g/cm^3 (Table 2). For example, at −95 °C, the density of the vapor CH_4 in the FSCC is 0.056 g/cm^3, and the density of the coexisting liquid phase is 0.284 g/cm^3. We can easily obtain the Raman spectra characteristics of high density CH_4 by this method. As shown in Figs. 4 and 6,

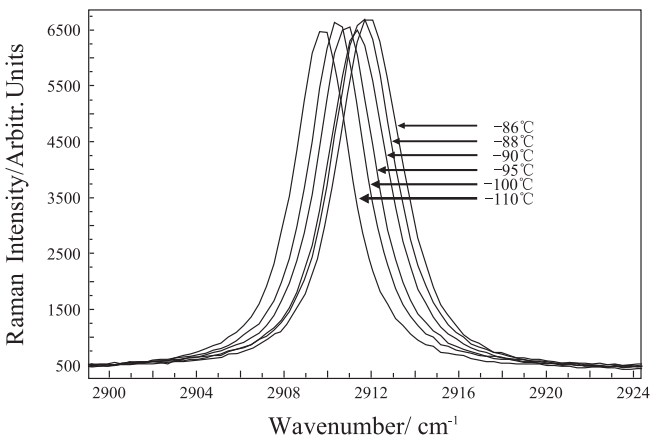

Figure 6. Raman spectra of liquid methane with various densities in a FSCC. The densities were defined by the set temperatures of the Linkam CAP 500 heating–cooling stage for the L-V coexisting CH_4 system in a FSCC.

the peak position of the C–H symmetric stretching band (ν_1) of methane shifts to lower wavenumbers as the density of liquid methane increases with the temperature decreasing, and shifts to higher wavenumbers as the density of methane vapor decreases with the temperature decreasing. These results are consistent with those from experiments using the HPOC method as shown in Fig. 4.

Conclusion

In this study, the positions of the CH_4 Raman ν_1 symmetric stretching bands were measured in a wide range of temperature (from −180 °C to 350 °C) and density (0.0007–0.45 g/cm^3). The position of this Raman band shifts systematically to lower wavenumbers with increasing density at constant temperature. At a given density, the peak shifts to lower wavenumbers with decreasing sample temperature. An equation was derived to describe the relationship among CH_4 ν_1 peak position, density, and temperature, and this equation can be applied to calculate the density of methane in a fluid inclusion from measured CH_4 ν_1 peak position at a fixed sample temperature on a heating–cooling stage.

Acknowledgements

We thank Professors Qiang Sun, Wanjun Lu, and Xi Liu for their advice on the processing and interpretation of Raman data. We also thank Dr. Guangfei Wei and Dr. Shuilong Wang for their help on the use the MATLAB software. We would like to acknowledge the support of Energy and Mineral Programs of US Geological Survey. Funding for this work was partly provided by grants from the 12th Five-Year Plan project of State Key Laboratory of Ore deposit Geochemistry, Chinese Academy of Sciences (SKLODG-ZY125-09), the Key Program of National Natural Science Foundation of China (41130432), the National Natural Science Foundation of China (40873051), the Knowledge Innovation Program (SIDSSE-201302) and the Hadal-trench Research Program (XDB06060100) of Chinese Academy of Sciences. The use of trade, product, industry, or firm names in this report is for descriptive purposes only and does not constitute endorsement by the US Government.

References

[1] F. Lin, A. K. Sum, R. J. Bodnar, *J. Raman Spectrosc.* **2007a**, *38*, 1510.
[2] F. Lin, R. J. Bodnar, S. P. Becker, *Geochim. Cosmochim. Acta* **2007b**, *71*, 3746.
[3] W. J. Lu, I. M. Chou, R. C. Burruss, Y. C. Song, *Geochim. Cosmochim. Acta* **2007**, *71*, 3969.
[4] X. L. Wang, I. M. Chou, W. X. Hu, R. C. Burruss, Q. Sun, Y. C. Song, *Geochim. Cosmochim. Acta* **2011**, *75*, 4080.
[5] J. Dubessy, S. Buschaert, W. Lamb, J. Pironon, R. Thiéry, *Chem. Geol.* **2001**, *173*, 193.
[6] J. Mullis, J. Dubessy, B. Poty, J. O'Neil, *Geochim. Cosmochim. Acta* **1994**, *71*, 2239.
[7] D. S. Kelley, J. A. Karson, G. L. Früh-Green, D. R. Yoerger, T. M. Shank, D. A. Butterfield, J. M. Hayes, M. O. Schrenk, E. J. Olson, G. Proskurowski, M. Jakuba, A. Bradley, B. Larson, K. Ludwig, D. Glickson, K. Buckman, A. S. Bradley, W. J. Brazelton, K. Roe, M. J. Elend, A. Delacour, S. M. Bernasconi, M. D. Lilley, J. A. Baross, R. E. Summons, S. P. Sylva, *Science* **2005**, *307*, 1428.
[8] D. S. Kelley, G. L. Früh-Green, *J. Geophys. Res.* **1999**, *104*(B5), 10439.
[9] D. Fabre, R. Couty, *C. R. Acad. Sci., Paris* **1986**, *303*(14), 1305.
[10] J. C. Seitz, J. D. Pasteris, I. M. Chou, *Am. J. Sci.* **1993**, *293*, 297.
[11] J. C. Seitz, J. D. Pasteris, I. M. Chou, *Am. J. Sci.* **1996**, *296*, 577.
[12] V. Thieu, S. Subramanian, S. O. Colgate, E. D. Sloan Jr., in Gas Hydrates: Challenges for the Future, (Eds: G. D. Holder, P. R. Bishnoi) Ann. N. Y. Acad. Sci, New York, **2000**, *912*, pp. 983.
[13] J. Pironon, J. O. W. Grimmer, S. Teinturier, D. Guillaume, J. Dubessy, *J. Geochem. Exploration.* **2003**, *78-79*, 111.
[14] M. A. Echargui, F. Marsault-Herail, *Mol. Phys.* **1987**, *60*, 605.
[15] I. M. Chou, R. C. Burruss, W. J. Lu, in Advances in High-Pressure Technology for Geophysical Applications, (Eds: J. Chen, Y. Wang, T. S. Duffy, G. Shen, L. F. Dobrzhinetakaya), Elsevier, Amsterdam, **2005**, pp. 475–485.
[16] I. M. Chou, Y. C. Song, R. C. Burruss, *Geochim. Cosmochim. Acta* **2008**, *72*, 5217.
[17] I. M. Chou, in Applications of Raman Spectroscopy to Earth Sciences and Cultureal Heritage: Chapter 6 in EMU Notes in Mineralogy (Eds: J. Dubessy, F. Rull). Vandoeuvre-Lès-Nancy, France, **2012**, pp. 227–247.
[18] S. Fukura, T. Mizukami, S. Odake, H. Kagi, *Appl. Spectrosc.* **2006**, *60*, 946.
[19] S. B. Hansen, R. W. Berg, E. H. Stenby, *Appl. Spectrosc.* **2001**, *55*, 745.
[20] D. Ben-Amotz, F. LaPlant, D. Shea, J. Gardecki, D. List, in *Supercritical Fluid Technology*: *ACS Symposium Series* 488 (Eds: F. Bright, M. P. McNally), American Chemical Society, Washington, DC, **1992**, pp. 18–30.
[21] D. Ben-Amotz, D. R. Herschbach, *J. Phys. Chem.* **1993**, *97*, 2295.
[22] I. M. Chou, X. L. Wang, R. C. Burruss, GeoRaman 10, **2012**, June 11-13, Nancy, France.